

LiNiO₂ as a high-entropy charge- and bond-disproportionated glass

Kateryna Foyevtsova*,^{1,2} Ilya Elfimov,^{1,2} Joerg Rottler,^{1,2} and George A. Sawatzky^{1,2}

¹*Department of Physics & Astronomy, University of British Columbia, Vancouver, BC V6T 1Z1, Canada*

²*Stewart Blusson Quantum Matter Institute, University of British Columbia, Vancouver, BC V6T 1Z4, Canada*

(Dated: January 31, 2022)

Understanding microscopic properties of LiNiO₂, a Li-ion battery cathode material with extraordinarily high reversible capacity, has remained a challenge for decades. Based on extensive electronic structure calculations, which reveal a large number of nearly degenerate phases involving local Jahn-Teller effect as well as bond and oxygen-based charge disproportionation, we propose that LiNiO₂ exists in a high-entropy charge-glass like state at and below ambient temperatures. Recognizing the glassy nature of LiNiO₂ does not only explain its key experimental features, but also opens a new path in designing entropy-stabilized battery cathodes with superb capacities.

PACS numbers: 61.43.Fs, 64.70.P-, 65.40.Gr, 71.20.-b, 75.47.Lx, 71.20.-b, 71.30.+h, 71.45.Lr

I. INTRODUCTION

LiNiO₂ is well known as a promising cathode material for rechargeable Li-ion batteries^{1,2}. One of the most fascinating but also puzzling properties of this oxide is its record-breaking stability upon repeated charge and discharge cycles. It is indeed quite surprising that the LiNiO₂ system can be cycled more than a few times changing the Li concentration by up to 80% on each cycle^{3,4}. This indicates that there must be something very special about the crystal structure of LiNiO₂ that keeps the original structure in place, and indeed LiNiO₂ has demonstrated a range of structural features that are hard to understand in a conventional way.

LiNiO₂ consists of layers of edge-sharing NiO₆ octahedra on a triangular lattice alternating with Li layers. The formally trivalent Ni ions are in a low-spin configuration $t_{2g}^6 e_g^1$ which makes them Jahn-Teller (JT) active^{2,5-7}. Despite this, however, the NiO₆ octahedra do not undergo a *cooperative* JT distortion even at the lowest temperatures, as follows from the numerous Rietveld refinements of the LiNiO₂ powder diffraction data^{2,4,8}. This is in a surprising contrast with the behavior of its sister compound NaNiO₂ that shows a ferro-orbital ordering of occupied d_{z^2} orbitals and an associated cooperative elongation of the NiO₆ octahedra below 460 K as illustrated in Fig. 1(a)^{9,10}. On the other hand, structural analyses based on the neutron pair distribution function (nPDF)⁸, extended x-ray absorption fine structure¹¹, and electron spin resonance^{12,13} measurements, strongly suggest *local*, but apparently *disordered*, Ni-O bond disproportionation in LiNiO₂. Disorder effects in this system, which also include a spin-glass-like behavior at low temperatures⁶, are often linked to its unavoidable deviation from stoichiometry^{4,14}. Yet, the exact nature of the disordered state in LiNiO₂ has so far remained unclear.

Apart from the above, LiNiO₂ also possesses a rather peculiar electronic property, which, although being often dismissed in literature, might be the key to understanding its structural properties. As was first pointed out by Kuiper *et al.*¹⁵, this system is in the negative

charge-transfer regime which brings the NiO₆ octahedra closer to the $(t_{2g}^6 e_g^2) \underline{L}$ (rather than the formal $t_{2g}^6 e_g^1$) *average* configuration, where \underline{L} denotes a ligand hole residing on a molecular orbital formed by the six oxygen- $2p_\sigma$ orbitals in an octahedron. In this regime, the Jahn-Teller effect might be in competition with another degeneracy lifting mechanism, observed in rare-earth nickel perovskites¹⁶⁻¹⁸, which involves formation of two types of size-disproportionated NiO₆ octahedra with configurations $t_{2g}^6 e_g^2$ and $(t_{2g}^6 e_g^2) \underline{L}^2$ with symmetries and spins corresponding to those of Ni²⁺ and Ni⁴⁺. Not surprisingly, therefore, a strongly competing bond-disproportionated phase of LiNiO₂, with ordered stripes of collapsed and expanded NiO₆ octahedra [Fig. 1(e)], was indeed recently predicted within density functional theory (DFT)¹⁹.

Our present theoretical study offers a unifying explanation of the puzzling structural and electronic properties of LiNiO₂ outlined above as well as its superior performance in Li-ion batteries by recognizing the fundamental role of entropy in this system. Based on extensive electronic structure calculations, we demonstrate that LiNiO₂ has a large number of nearly degenerate states involving NiO₆ octahedra with $t_{2g}^6 e_g^2$, $(t_{2g}^6 e_g^2) \underline{L}$ and $(t_{2g}^6 e_g^2) \underline{L}^2$ configurations, leading to basically a large number of combinations of these into glassy-like structures which increases the entropy resulting in a high-entropy material. It is shown that, as a result of the charge-transfer energy being negative in LiNiO₂, this state involves charge disproportionation on oxygen rather than on nickel atoms. Although entropy is known to play important roles in polymer science and protein folding as well as glasses, multi-component oxides, and metal alloys^{20,21}, these are mostly structurally driven while our proposal involves an electronic-structure driven mechanism for the pure material.

II. METHODS

We performed density functional theory (DFT) calculations with the pseudo-potential code VASP^{22,23} and the

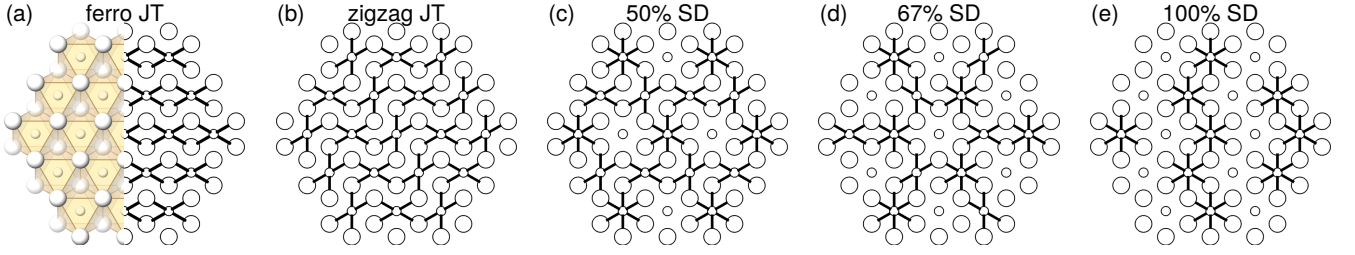


FIG. 1: Possible orderings of short and long Ni-O bonds in the triangular lattice of NiO_6 octahedra. Nickel (oxygen) atoms are represented by small (large) circles. The short Ni-O bonds are shown as black connecting lines. In (a), a three-dimensional view of the lattice is shown on the left-hand side for a reference. Panels (a) and (b) represent phases where only Jahn-Teller (JT) distorted NiO_6 octahedra are present, whereas panels (c), (d), and (e) represent phases where, respectively, 50%, 67%, and 100% of the NiO_6 octahedra are size-disproportionated (SD).

all-electron code WIEN2k²⁴. All of our structural relaxations were done in VASP, using a high energy cut-off of 550 Ry and fine k -grids with densities close to that of a $12 \times 12 \times 12$ k -grid in a $5.5 \text{ \AA} \times 5.5 \text{ \AA} \times 5.5 \text{ \AA}$ unit cell. A combination of the local density approximation (LDA)²⁵ and the LDA+U method as designed by Anisimov *et al.*^{26–28}, with the Ni-3d electrons' on-site interactions $U = 6$ eV and $J_H = 1$ eV, was used to treat exchange and correlation effects.

The neutron pair distribution functions (nPDF), $G(r)$, of the relaxed LiNiO_2 phases were simulated with the PDFfit2 program²⁹ using the following expression⁸:

$$G(r) = \frac{1}{rN} \sum_{i,j} \left[\frac{b_i b_j}{\langle b \rangle^2} \delta(r - r_{ij}) \right] - 4\pi\rho_0,$$

where r is distance, b_i and r_{ij} are the scattering length of the i th atom and the distance between the i th and j th atom, respectively, N is the number of atoms, and ρ_0 is the average atomic density. Thermal broadening was accounted for through introducing the Debye-Waller factors. We used theoretical structural parameters, scaled with an empirical factor of 1.024, and theoretical thermal displacement parameters. In the PDFfit2 program, we chose 0.08 for the Q_{damp} parameter and 0.5 for the linear atomic correlation factor δ_1 for all the considered model LiNiO_2 phases except the rhombohedral one where we used $\delta_1 = 0.2$. The neutron time-of-flight (TOF) powder diffraction patterns were simulated using the GSAS package^{30,31}. For both the nPDF and the TOF powder diffraction simulations, we used the following theoretically calculated atomic isotropic displacement parameters $U \equiv U_{11} = U_{22} = U_{33}$, obtained for the temperature of 10 K employing VASP and the Phonopy package³²: $U(\text{Li}) = 0.008 \text{ \AA}^2$, $U(\text{Ni}) = 0.0011 \text{ \AA}^2$, $U(\text{O}) = 0.0025 \text{ \AA}^2$. The thermodynamic properties were calculated using the phonon spectra obtained with VASP and Phonopy via the dynamical matrix method.

III. RESULTS

Our following discussion will be based on a comparison of a number of different bond-disproportionated phases of LiNiO_2 shown in Fig. 1, which all turn out to be easily achievable in a DFT structural relaxation. They include two JT phases [(a) and (b)], the stripy phase with size-disproportionated NiO_6 octahedra from Ref. 19 (e), and two mixed phases where JT-distorted and size-disproportionated octahedra are simultaneously present [(c) and (d)]. The high-symmetry rhombohedral $R\bar{3}m$ phase of LiNiO_2 , which has been traditionally assigned to LiNiO_2 based on powder diffraction refinement and has no Ni-O bond disproportionation, will also be considered for completeness. For each phase, we use DFT and the local density approximation +U (LDA+U) method to perform full lattice relaxation and to calculate the ground state electronic structure. Ferromagnetic alignment of Ni spins is adopted throughout all the calculations, as it was established that the total energy differences between different spin configurations are much smaller than those between the different structural phases of LiNiO_2 , as detailed in the Appendix. This finding of ours agrees with the conclusions of Mostovoy and Khomskii³³ who demonstrated decoupling of spin and orbital degrees of freedom in LiNiO_2 .

We note first that for NaNiO_2 (the sister compound) DFT correctly predicts the JT phase with a ferro-orbital ordering of occupied d_{z^2} orbitals [Fig. 1(a)] to be the lowest energy state^{19,34}. For LiNiO_2 , on the other hand, we find that the lowest energy state is the JT phase with a zigzag ordering of occupied d_{z^2} orbitals [Fig. 1(b)]¹⁹. Its energy is by 18.1 meV per formula unit (f. u.) lower than that of the ferro-orbitally ordered phase and by 141.3 meV/f. u. lower than that of the rhombohedral phase (see Table I). The fully and partially size-disproportionated (SD) phases shown in Figs. 1(c)-(e) have energies that are not too far from the energy of the ferro-orbital JT phase. For example, the three-fold rotationally symmetric phase shown in (d), with two thirds (or 67%) of Ni sites being SD, is higher in energy by

Phase	E_{tot} (meV/f. u.)	Gap (eV)	$N_{\text{short}}/N_{\text{long}}$	$d_{\text{Ni-O}}$ (Å)
Rhomb.	141.3 (147.5)	0	-	1.98
ferro JT	18.1 (0)	0.43	2	1.90 2.12
zigzag JT	0 (19.1)	0.56	2	1.90 2.11
50% SD	49.6 (60.1)	0.35	1.4	1.90 2.06
67% SD	32.1 (43.5)	0.51	1.25	1.90 2.05
100% SD	26.3 (63.3)	0.58	1	1.89 2.06

TABLE I: Calculated properties of the LiNiO_2 model phases. E_{tot} are relative total energies, $N_{\text{short}}/N_{\text{long}}$ are the ratios of the numbers of short and long Ni-O bonds, and $d_{\text{Ni-O}}$ are the average nearest-neighbor Ni-O bond lengths. A scaling factor of 1.024 has been applied to the original $d_{\text{Ni-O}}$ values obtained within LDA+U. For comparison, E_{tot} values relevant for NaNiO_2 are provided in parentheses.

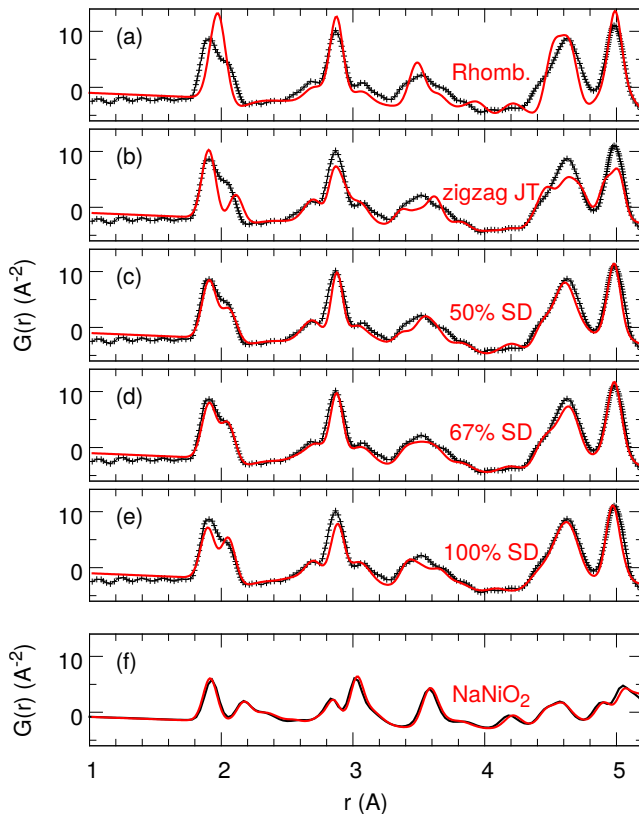


FIG. 2: Neutron pair distribution functions (nPDF) $G(r)$ of LiNiO_2 and NaNiO_2 . In (a)-(e), the experimental (black symbols)⁸ and various theoretically simulated (red lines) nPDFs at the temperature of 10 K are compared for LiNiO_2 . Panel (f) shows nPDFs of NaNiO_2 simulated using its experimental crystal structure (black line)¹⁰ and using a relaxed structure from LDA+U calculations (red line). A scaling factor of 1.024 has been applied to r in $G(r)$ calculated using results of LDA+U structural relaxations.

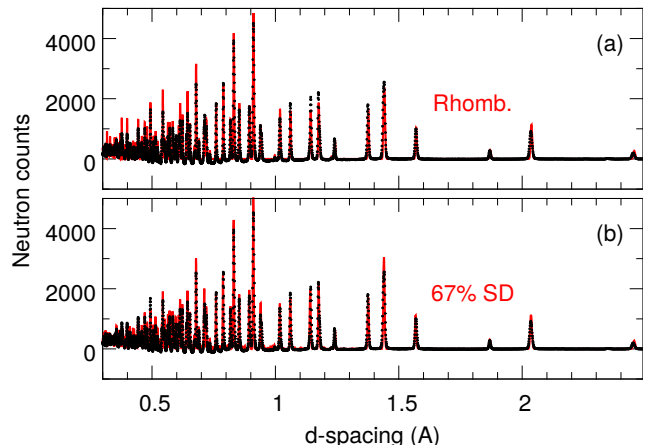


FIG. 3: Neutron time-of-flight powder diffractograms of LiNiO_2 . Experiment (black symbols)⁸ is compared to a simulation (red lines) where (a) the rhombohedral and (b) the 67% SD model phase of LiNiO_2 at 10 K is used. A scaling factor of 1.024 has been applied to the d -spacing in the simulated diffractograms.

only 14 meV/f. u. As one can also see in Table I, all the considered bond-disproportionated phases have a small charge gap in LDA+U, which qualitatively agrees with experiment⁶. Interestingly, the same SD phases can be obtained for NaNiO_2 , but, as also shown in Table I, they are energetically more strongly removed from the lowest energy state than in the case of LiNiO_2 .

Before discussing the important implications following from these total energy calculations, let us point out that LiNiO_2 being in a mixed phase, such as the 67% SD one, could explain amazingly well the findings from both, the pair distribution function and the powder diffraction analyses, which previously have been regarded as mutually contradicting. In Figs. 2(a)-(e), the experimental nPDF of LiNiO_2 ⁸ is compared with simulated nPDFs of the five model phases from Fig. 1. Both the experiment and the simulations are performed at the temperature of 10 K. In order to correct for the underestimation of interatomic distances in LDA+U, an empirical scaling factor of 1.024 was applied to r in the simulated nPDF $G(r)$. This procedure gives very good agreement between theory and experiment for NaNiO_2 , whose experimental crystal structure is unambiguously known [Fig. 2(f)]¹⁰. For LiNiO_2 , it is the 67% SD phase's nPDF that has equally good agreement with experiment [Fig. 2(d)], while the zigzag JT (lowest energy state) phase's nPDF shows considerable deviations [Fig. 2(b)]. In the bond-disproportionated phases [Figs. 2(b)-(e)], the two nPDF peaks around 2 Å are particularly sensitive to the presence of SD NiO_6 sites and their evolution from (b) to (e) is easy to understand. Indeed, the relative heights of these peaks reflect the ratio between the numbers of short and long nearest-neighbor Ni-O bonds, $N_{\text{short}}/N_{\text{long}}$. As the fraction of SD sites grows,

$N_{\text{short}}/N_{\text{long}}$ gradually decreases from 2 in the fully JT phases to 1 in the fully SD phase (Table I) and so does the intensity of the first nPDF peak relative to that of the second. Furthermore, only by having SD sites in the system can one accurately reproduce the measured position of the second peak or, equivalently, the average length of the long Ni-O bonds (Table I). We would like to emphasize that these results have been obtained with keeping the nPDF simulations as *ab initio* as possible, which is a step forward compared with the original analysis of Chung *et al.* in Ref. 8. We also note that, in general, the fraction of SD octahedra may probably vary from one sample to another depending on their thermal histories and growth conditions, which should be a subject of further investigations.

As for the powder diffraction experiments, we find that the 67% SD phase gives a diffraction pattern that is strikingly similar to that of the rhombohedral phase (Fig. 3). Moreover, our general observation is that all bond-disproportionated phases with a preserved C_3 symmetry of the lattice tend to have very similar diffraction patterns³⁵. In other words, the powder diffraction pattern of LiNiO_2 appears to be barely sensitive to Ni-O bond disproportionation as long as the C_3 symmetry is preserved, which in fact can explain the long-standing confusion around the LiNiO_2 crystal structure.

IV. DISCUSSION

A. Role of entropy

At this point, the question arises as to why LiNiO_2 would adopt a metastable phase like the 67% SD one rather than the lowest energy JT zigzag phase, which is what the above comparison with experiment strongly suggests, and this is where the entropy factor comes into play. In fact, given the accuracy limitations of the LDA+U method, the only robust conclusion that comes from our total energy calculations is that there exist phases with varying amounts of JT distorted and SD NiO_6 octahedra whose energies lie within only 20 to 30 meV/f. u. above the ground-state energy. While the ferro JT, 67% SD, 50% SD, and 100% SD phases are just some examples of such phases, further examples can be easily come up with and tested in a calculation by exploring various ways of positioning the five *building block* configurations of a NiO_6 octahedron on a triangular lattice: the three JT distorted and the two SD configurations [Fig. 4(a)]. With so many metastable phases being so close in energy, a state where the system is able to fluctuate between them can have a high enough entropy to be stabilized at ambient temperatures by the entropy term in the free energy. In this fluctuating state, each NiO_6 site can assume any of the building block configurations, and in an extreme limit would do it in a random way. In reality, of course, there will be constraints due to local correlations between different types of sites mostly deter-

mined by Pauling's principle of electroneutrality³⁶. Thus, an expanded NiO_6 octahedral site with electronic configuration d^8 would "attract" collapsed $d^8\bar{L}^2$ sites (each having 2e less charge due to the 2 ligand holes than the reference d^8 site) in its immediate vicinity, but due to the triangular geometry those will be somehow diluted by $d^8\bar{L}$ and/or d^8 sites. One can envision this mechanism driving a propagation of local d^8 , $d^8\bar{L}$, and $d^8\bar{L}^2$ configurations from a nucleation center ensured by the entropy to be as random as possible at a given temperature. We believe that the final entropy-stabilized state will involve local distributions of d^8 , $d^8\bar{L}$, and $d^8\bar{L}^2$ sites corresponding to all and any of those depicted in Fig. 1. We can in fact make the discussion more quantitative by computing and comparing the configurational entropy of this entropy-stabilized state and that of the lowest-energy zigzag Jahn-Teller phase. As detailed in the Appendix, the impact of the vibrational (or phonon) free energy F^{phon} on the stability of various LiNiO_2 phases is small compared to that of the configurational entropy and therefore will not be considered here. The configurational entropy of the zigzag Jahn-Teller phase is due to spin fluctuations between the $S_z = \pm\frac{1}{2}$ states of the Ni ions' spins: $S^{\text{conf}} = Nk_B \ln 2 = 0.693Nk_B$, where N is the number of formula units in the crystal. For the entropy-stabilized state, let us assume for simplicity that the d^8 , $d^8\bar{L}$, and $d^8\bar{L}^2$ sites have equal concentrations of 1/3, and that they are randomly distributed. In addition, the JT $d^8\bar{L}$ sites have degeneracy of $g_1 = 6$ corresponding to three possible orientations of the long Ni-O bond [see Fig. 4(a)] and two S_z components of spin $S = \frac{1}{2}$, while the large octahedron sites d^8 have degeneracy of $g_2 = 3$ corresponding to three S_z components of spin $S = 1$. Neglecting local correlations between the different types of sites, which otherwise would somewhat reduce our estimate of S^{conf} , we get that $S^{\text{conf}} = k_B \ln(3^N (g_1^{N/3} g_2^{N/3})) = 2.062Nk_B$. This upper bound is in fact very large and exceeds the value of $\ln 5 = 1.61$ in five-component mixtures at equal concentrations, which are conventionally considered "high-entropy" materials³⁷. We note that, aside from the chemical composition aspects used in the design of high-entropy alloys^{20,38}, our analysis puts a new twist on the determination of the entropy to include Jahn-Teller as well as electronic and local disproportionation.

It would be very interesting to look for experimental signatures of the glass transition in LiNiO_2 , at which the electronic and orbital fluctuations discussed above should freeze. For example, it was found that the heat capacity of LiNiO_2 is anomalously enhanced below 300 K³⁹. Clearly, further heat capacity measurements exploring much higher temperatures are strongly desired in order to observe the full glass transition. Another experimental observation which is strongly supportive of the glassy state in LiNiO_2 is the spin-glass like transition observed at around 20 K. Indeed, having the Ni sites electronically in a random mixture of $d^7\bar{L}$, $d^8\bar{L}^2$, and d^8 configurations means having a random mixture of $S = \frac{1}{2}$, $S = 0$, and

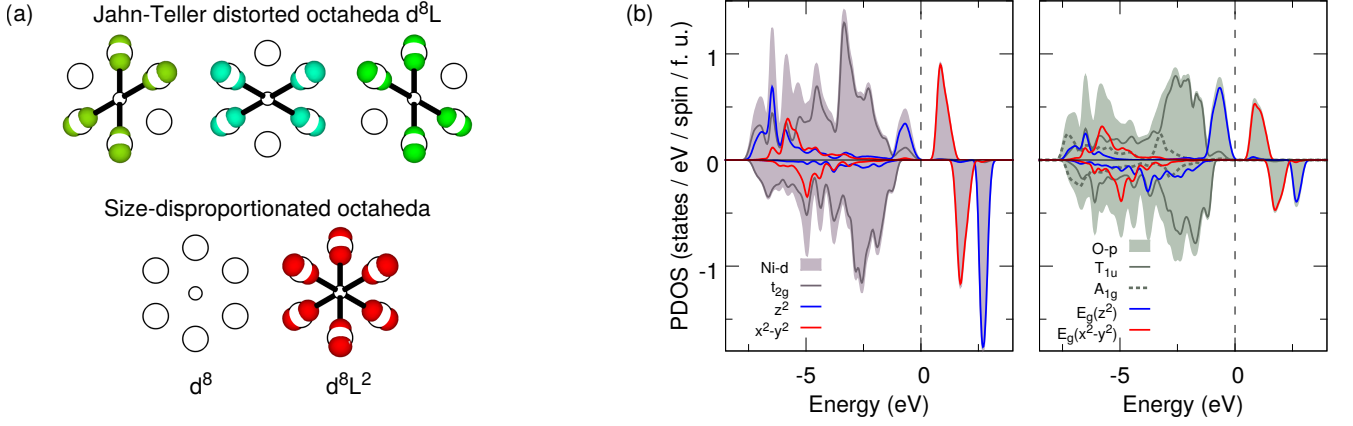


FIG. 4: (a) The five building block configurations of the NiO_6 octahedra in LiNiO_2 : the three JT distorted configurations and the two SD configurations. In color shown are the density iso-surfaces of holes occupying E_g oxygen molecular orbitals. (b) Orbitaly projected densities of states (PDOS) in the zigzag JT phase of LiNiO_2 . The right panel features projections onto oxygen molecular orbitals of various symmetries. Both plots are normalized to a single NiO_6 octahedron with only $\text{O-}p_\sigma$ orbitals participating.

$S = 1$ spin magnetic moments, respectively, with similarly randomized exchange interactions between them, which is an important prerequisite for the formation of a spin glass.

From the application point of view, the high configurational entropy of the glassy state in LiNiO_2 is very beneficial in terms of battery operation as the system has many ways to adjust itself locally to a missing Li ion, which is apparently what makes LiNiO_2 such a good cathode. In this regard, further increase of entropy upon chemical substitution of Ni with Co and Mn may be the main reason for the increased stability of $\text{LiNi}_{1-x-y}\text{Co}_x\text{Mn}_y\text{O}_2$ cathodes. Another example of this concept can be found in a recent study on multi-component monoxides which demonstrates that five-component systems perform much better in batteries compared with four- or less component systems and attributes this effect to entropy stabilization³⁸.

B. Oxygen holes

Finally, in order to better understand the microscopic nature of the disordered glassy state in LiNiO_2 , let us examine its electronic structure. We first note that LDA+U correctly describes LiNiO_2 as a negative charge-transfer system¹⁵, as far as the Ni oxidation state is concerned. Figure 4(b) compares the Ni-3d and O-2p orbitaly projected densities of states (DOS) in the zigzag JT phase. One can see a considerable amount of the O-2p character in the states above the Fermi level, indicating that the true Ni oxidation state is far less than 3+. We find close to 8 electrons in the Ni-3d shell inside the muffin-tin sphere. What obscures the picture, though, is the strong hybridization between the Ni- e_g orbitals and the oxygen-2p orbitals of a respective symmetry. As one can see in the right panel of Fig. 4(b), it results in holes oc-

cupying E_g -symmetric molecular-like orbitals formed by the oxygen- $2p_\sigma$ orbitals in an octahedral cage. Although LDA+U is a mean-field method not capable of properly describing a many-body wave-function, we still can associate the states observed in our calculations on the expanded, JT distorted, and collapsed octahedra with, respectively, the $t_{2g}^6 e_g^2$, $(t_{2g}^6 e_g^2)\underline{L}$, and $(t_{2g}^6 e_g^2)\underline{L}^2$ configurations. Hole density iso-surfaces for each configuration are schematically shown in Fig. 4(a). Note that a single hole occupying the $x^2 - y^2$ -symmetric E_g molecular orbital results in a *shortening* of only four Ni-O bonds, while two holes occupying both the $x^2 - y^2$ - and the z^2 -symmetric E_g orbitals result in a *collapse* of all Ni-O bonds. We further find 1.68, 0.90, and 0.08 μ_B for the magnetic moments of the Ni ions inside the expanded, JT distorted, and collapsed octahedra, respectively. Again, this is a result of LDA+U being a mean-field method; in a true many-body calculation, one would find for $(t_{2g}^6 e_g^2)\underline{L}^2$, for example, that the $S = 1$ moment on the nickel forms a singlet state with the $S = 1$ moment on the oxygen molecular orbital and the total moment on the octahedron is zero.

Yet another peculiar property of the SD phases in LiNiO_2 is that there occur both bond disproportionation and *oxygen charge disproportionation*. This is in contrast with the rare-earth nickel perovskites, where only *bond disproportionation* occurs, which is a result of a different lattice geometry and a different average number of holes per oxygen octahedron (three in LiNiO_2 versus two in the rare-earth nickel perovskites). In Fig. 5(a), we schematically show density iso-surfaces of holes occupying individual molecular orbitals in the 67% SD phase of LiNiO_2 . One can clearly distinguish oxygen sites where neighboring molecular orbitals overlap from those where they do not. As a result, the two types of oxygen sites have different hole concentrations, which is further illustrated in Fig. 5(b).

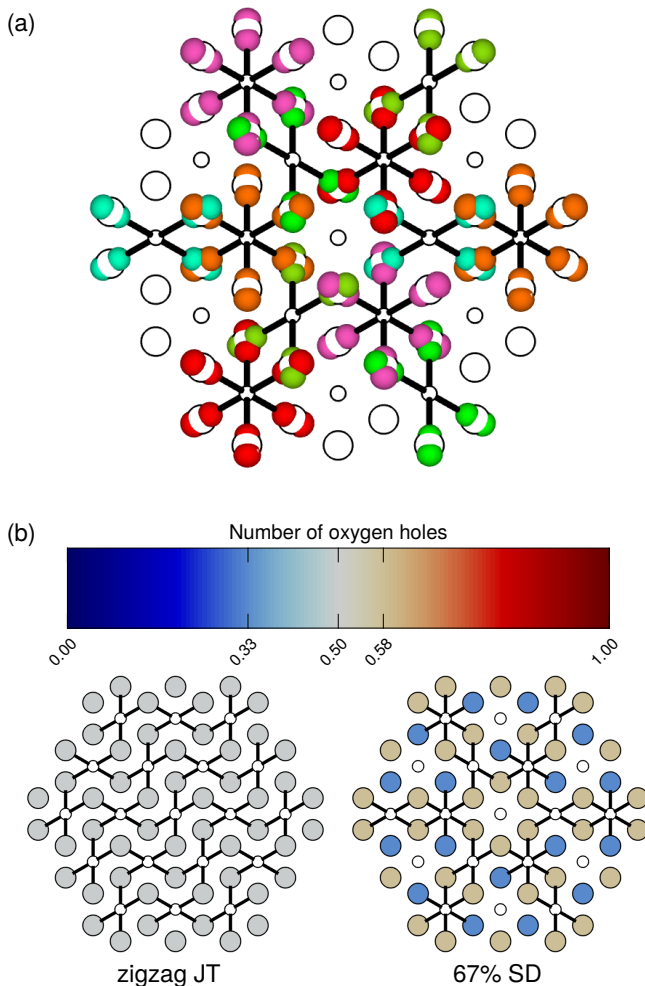


FIG. 5: Oxygen charge disproportionation in LiNiO₂. (a) A schematic illustration of the density iso-surfaces of holes occupying individual oxygen molecular orbitals in the 67% SD phase. (b) Oxygen charge disproportionation in the 67% SD phase versus a homogeneous hole distribution in the zigzag JT phase.

The extended nature of the oxygen molecular orbitals and the fact that they can overlap result in a strong nearest-neighbor interaction between holes, which is generally known to facilitate charge ordering effects. Although formation of a glassy state may in general depend on various factors, we can speculate that in such an environment localized charge impurities can serve as nucleation centers for charge disproportionation. In LiNiO₂, charge impurities are readily available in a form of doped electrons entering the Ni layers as a result of the unavoidable deviation from stoichiometry⁴. The doped electrons would attract holes according to Pauling's principle³⁶ and thus locally modify the energetics in favor of charge- (and size-) disproportionated phases. Further investigations are, however, required in order to validate this scenario.

We believe that spectroscopic probes, such as x-ray

absorption spectroscopy (XAS), could be crucial in verifying the mixed size-disproportionated state in LiNiO₂. Especially interesting would be to compare spectroscopic data from LiNiO₂ and its sister compound NaNiO₂ where the ground state is contrastingly uniform. Unfortunately, unambiguous interpretation of the existing Ni 2*p* XAS data^{40–42} is not easy due to questionable sample quality and also the fact that their proper theoretical description requires to go beyond the standard single cluster calculations¹⁷. We hope therefore that our theoretical proposal of the glass-like electronic ground state of LiNiO₂ will stimulate experimental efforts in preparing and systematically measuring high-quality LiNiO₂ and NaNiO₂ samples complemented with a proper theoretical analysis of spectroscopic data in the spirit of Ref. 17. We also note that in the case of the negative charge-transfer gap rare-earth nickelates the detailed analysis of their XAS data identifying the origin of the two-peak structure was only made after the single crystalline epitaxial thin film studies with resonant inelastic x-ray scattering by Bisogni *et al.*⁴³. This kind of study on epitaxial thin films of LiNiO₂ and NaNiO₂ would be extremely helpful.

V. CONCLUSION

In summary, we have used electronic structure methods to demonstrate that the Li-ion battery material LiNiO₂ is in a high-entropy charge-glass like state characterized by a disordered mixture of JT distorted and SD NiO₆ octahedra. This state is associated with charge disproportionation on the oxygen rather than on the nickel atoms due to LiNiO₂ being in the negative charge-transfer regime. Supported by rigorous calculations, our proposal explains the previously highly debated nPDF and powder diffraction measurements on LiNiO₂ as well as its enhanced heat capacity and the spin-glass like behavior. Most importantly, however, we can conclude that it is the glassy nature that renders LiNiO₂ its extraordinarily high reversible capacity. We believe that recognizing the role of entropy in stabilizing cathodes during the charge and discharge cycles can greatly advance battery research.

Appendix

A. Dependence of energy on a spin configuration

Figure 6 demonstrates that the energy differences between different structural phases of LiNiO₂ are very weakly dependent on the Ni spin configuration. In this plot, we have considered the zigzag JT, ferro-orbital JT, and fully size-disproportionated structural phases as well as one ferromagnetic and three anti-ferromagnetic Ni spin configurations labeled as FM, AFM1, AFM2, and AFM3.

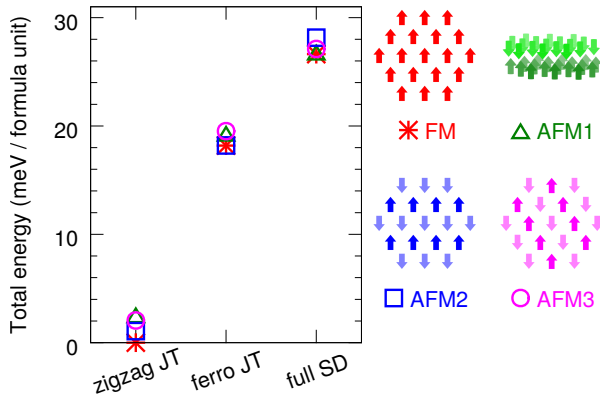


FIG. 6: Relative total energies as a function of a structural phase and Ni spin configuration in LiNiO_2 . FM stands for the ferromagnetic spin configuration. The anti-ferromagnetic configuration AFM1 corresponds to alternating layers of up and down spins. The anti-ferromagnetic configurations AFM2 and AFM3 correspond to two different arrangements of up and down spins within a layer. Note that AFM2 and AFM3 are not equivalent due to the broken C_3 symmetry in the considered structural phases.

B. Calculation of thermodynamic properties

In order to estimate how important is the impact of the vibrational free energy on the stability of various LiNiO_2

phases, we have computed the vibrational free energies $F^{\text{phon}} = E^{\text{phon}} - TS^{\text{phon}}$ of the zigzag JT and the 67% SD phases of LiNiO_2 using the phonon spectra obtained with VASP and Phonopy via the dynamical matrix method. The computed vibrational entropies S^{phon} , the harmonic phonon energies E^{phon} , as well as the total entropies and total free energies $F = E^{T=0} + F^{\text{phon}} - TS^{\text{conf}}$ are shown in Fig. 7 as a function of temperature T . $E^{T=0}$ is the $T = 0$ energy, which is 0 and +32.1 meV/f.u. in the zigzag JT and the 67% SD phases, respectively. It is assumed that the configurational entropy of the 67% SD phase is that of the entropy-stabilized state with equal concentrations of d^8 , $d^8\bar{L}$, and $d^8\bar{L}^2$ sites in order to illustrate its significant contribution compared with the phonon contribution.

Acknowledgments

The authors are grateful to Daniel Khomskii for insightful discussions. K. F. thanks Jae-Ho Chung and Thomas E. Proffen for sharing their neutron data and Leopoldo Suescun for helping with GSAS simulations.

- ¹ J. B. Goodenough, Phys. Rev. **100**, 564 (1955).
- ² J. B. Goodenough, J. Phys. Chem. Solids **6**, 287 (1958).
- ³ W. Liu, P. Oh, X. Liu, M.-J. Lee, W. Cho, S. Chae, Y. Kim, and J. Cho, Angewandte Chemie International Edition **54**, 4440 (2015), ISSN 1521-3773, URL <http://dx.doi.org/10.1002/anie.201409262>.
- ⁴ H. Arai, S. Okada, H. Ohtsuka, M. Ichimura, and J. Yamaki, Solid State Ionics **80**, 261 (1995), ISSN 0167-2738.
- ⁵ K. Hirakawa, H. Kadowaki, and K. Ubukoshi, Journal of the Physical Society of Japan **54**, 3526 (1985), <http://dx.doi.org/10.1143/JPSJ.54.3526>, URL <http://dx.doi.org/10.1143/JPSJ.54.3526>.
- ⁶ K. Hirota, Y. Nakazawa, and M. Ishikawa, Journal of Physics: Condensed Matter **3**, 4721 (1991), URL <http://stacks.iop.org/0953-8984/3/i=25/a=017>.
- ⁷ K. Yamaura, M. Takano, A. Hirano, and R. Kanno, Journal of Solid State Chemistry **127**, 109 (1996), ISSN 0022-4596, URL <http://www.sciencedirect.com/science/article/pii/S0022459696903631>.
- ⁸ J.-H. Chung, T. Proffen, S. Shamoto, A. M. Ghorayeb, L. Croguennec, W. Tian, B. C. Sales, R. Jin, D. Mandrus, and T. Egami, Phys. Rev. B **71**, 064410 (2005), URL <http://link.aps.org/doi/10.1103/PhysRevB.71.064410>.
- ⁹ P. Borgeers and U. Enz, Solid State Communications **4**, 153 (1966), ISSN 0038-1098, URL <http://www.sciencedirect.com/science/article/pii/0038109866900019>.
- ¹⁰ M. Holzapfel, S. de Brion, C. Darie, P. Bordet, E. Chappel, G. Chouteau, P. Strobel, A. Sulpice, and M. D. Núñez Regueiro, Phys. Rev. B **70**, 132410 (2004), URL <http://link.aps.org/doi/10.1103/PhysRevB.70.132410>.
- ¹¹ A. Rougier, C. Delmas, and A. Chadwick, Solid State Communications **94**, 123 (1995), ISSN 0038-1098, URL <http://www.sciencedirect.com/science/article/pii/0038109895000208>.
- ¹² A.-L. Barra, G. Chouteau, A. Stepanov, A. Rougier, and C. Delmas, The European Physical Journal B - Condensed Matter and Complex Systems **7**, 551 (1999), ISSN 1434-6036, URL <https://doi.org/10.1007/s100510050648>.
- ¹³ F. Reynaud, D. Mertz, F. Celestini, J.-M. Debierre, A. M. Ghorayeb, P. Simon, A. Stepanov, J. Voiron, and C. Delmas, Phys. Rev. Lett. **86**, 3638 (2001), URL <http://link.aps.org/doi/10.1103/PhysRevLett.86.3638>.
- ¹⁴ L. Petit, G. M. Stocks, T. Egami, Z. Szotek, and W. M. Temmerman, Phys. Rev. Lett. **97**, 146405 (2006), URL <https://link.aps.org/doi/10.1103/PhysRevLett.97.146405>.
- ¹⁵ P. Kuiper, G. Kruizinga, J. Ghijsen, G. A. Sawatzky, and H. Verweij, Phys. Rev. Lett. **62**, 221 (1989), URL <http://link.aps.org/doi/10.1103/PhysRevLett.62.221>.
- ¹⁶ S. Johnston, A. Mukherjee, I. Elfimov, M. Berciu, and G. A. Sawatzky, Phys. Rev. Lett. **112**, 106404 (2014), URL <http://link.aps.org/doi/10.1103/PhysRevLett.112.106404>.
- ¹⁷ R. J. Green, M. W. Haverkort, and G. A. Sawatzky, Phys. Rev. B **94**, 195127 (2016), URL <https://link.aps.org/>

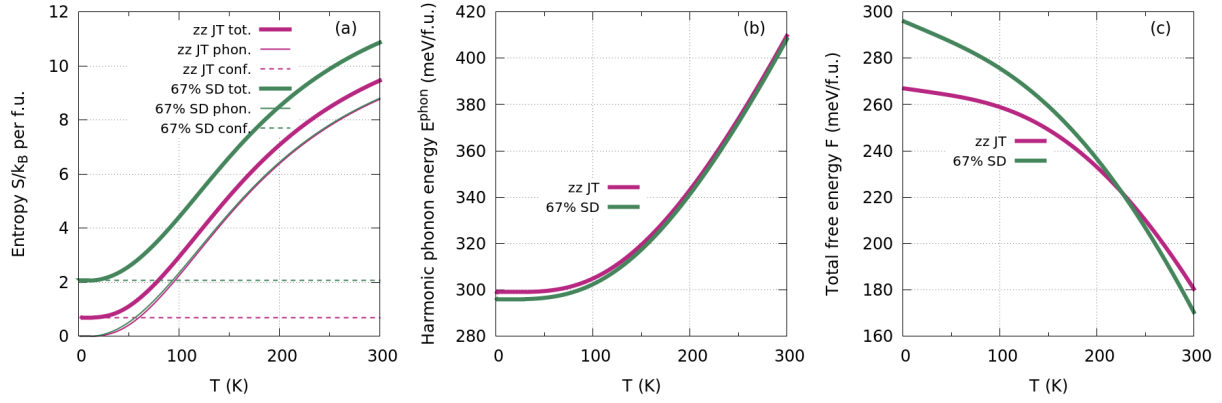


FIG. 7: Temperature dependence of the thermodynamic properties of LiNiO₂ in the zigzag Jahn-Teller (zz JT) and the 67% size-disproportionated (67% SD) phases: (a) configurational, vibrational, and total entropies S ; (b) harmonic phonon energy E^{phon} ; (c) total free energy F .

- doi/10.1103/PhysRevB.94.195127.
- ¹⁸ K. Foyevtsova, A. Khazraie, I. Elfimov, and G. A. Sawatzky, *Phys. Rev. B* **91**, 121114 (2015), URL <http://link.aps.org/doi/10.1103/PhysRevB.91.121114>.
 - ¹⁹ H. Chen, C. L. Freeman, and J. H. Harding, *Phys. Rev. B* **84**, 085108 (2011), URL <http://link.aps.org/doi/10.1103/PhysRevB.84.085108>.
 - ²⁰ C. M. Rost, E. Sachet, T. Borman, A. Moballegh, E. C. Dickey, D. Hou, J. L. Jones, S. Curtarolo, and J.-P. Maria, *Nature Communications* **6**, 8485 (2015).
 - ²¹ Y. Yao, Z. Huang, P. Xie, S. D. Lacey, R. J. Jacob, H. Xie, F. Chen, A. Nie, T. Pu, M. Rehwoldt, et al., *Science* **359**, 1489 (2018), ISSN 0036-8075, <http://science.sciencemag.org/content/359/6383/1489.full.pdf>, URL <http://science.sciencemag.org/content/359/6383/1489>.
 - ²² G. Kresse and J. Furthmüller, *Computational Materials Science* **6**, 15 (1996), ISSN 0927-0256, URL <http://www.sciencedirect.com/science/article/pii/S0927025696000080>.
 - ²³ J. Paier, R. Hirschl, M. Marsman, and G. Kresse, *The Journal of Chemical Physics* **122**, 234102 (2005), URL <http://scitation.aip.org/content/aip/journal/jcp/122/23/10.1063/1.1926272>.
 - ²⁴ P. Blaha, K. Schwarz, G. K. H. Madsen, D. Kvasnicka, and J. Luitz, *WIEN2K, An Augmented Plane Wave + Local Orbitals Program for Calculating Crystal Properties* (Karlheinz Schwarz, Techn. Universität Wien, Austria, 2001).
 - ²⁵ J. P. Perdew and Y. Wang, *Phys. Rev. B* **45**, 13244 (1992), URL <http://link.aps.org/doi/10.1103/PhysRevB.45.13244>.
 - ²⁶ V. I. Anisimov, J. Zaanen, and O. K. Andersen, *Phys. Rev. B* **44**, 943 (1991), URL <http://link.aps.org/doi/10.1103/PhysRevB.44.943>.
 - ²⁷ V. I. Anisimov, I. V. Solovyev, M. A. Korotin, M. T. Czyżyk, and G. A. Sawatzky, *Phys. Rev. B* **48**, 16929 (1993), URL <http://link.aps.org/doi/10.1103/PhysRevB.48.16929>.
 - ²⁸ A. I. Liechtenstein, V. I. Anisimov, and J. Zaanen, *Phys. Rev. B* **52**, R5467 (1995), URL <http://link.aps.org/doi/10.1103/PhysRevB.52.R5467>.
 - ²⁹ C. L. Farrow, P. Juhas, J. W. Liu, D. Bryndin, E. S. Božin, J. Bloch, T. Proffen, and S. J. L. Billinge, *Journal of Physics: Condensed Matter* **19**, 335219 (2007), URL <http://stacks.iop.org/0953-8984/19/i=33/a=335219>.
 - ³⁰ A. Larson and R. V. Dreele, Los Alamos National Laboratory Report LAUR **86**, 748 (2000).
 - ³¹ B. H. Toby, *J. Appl. Cryst.* **34**, 210 (2001).
 - ³² A. Togo and I. Tanaka, *Scr. Mater.* **108**, 1 (2015).
 - ³³ M. V. Mostovoy and D. I. Khomskii, *Phys. Rev. Lett.* **89**, 227203 (2002), URL <http://link.aps.org/doi/10.1103/PhysRevLett.89.227203>.
 - ³⁴ H. Meskine and S. Satpathy, *Journal of Applied Physics* **97**, 10A314 (2005), <https://doi.org/10.1063/1.1854414>, URL <https://doi.org/10.1063/1.1854414>.
 - ³⁵ For instance, such is a JT phase where the direction of the long Ni-O bond in an octahedron alternates between successive layers.
 - ³⁶ L. Pauling, *J. Chem. Soc.* pp. 1461–1467 (1948), URL <http://dx.doi.org/10.1039/JR9480001461>.
 - ³⁷ B. S. Murty, J.-W. Yeh, and S. Ranganathan, *High-entropy alloys* (Butterworth-Heinemann, 2014).
 - ³⁸ A. Sarkar, L. Velasco, D. Wang, Q. Wang, G. Talasila, L. de Biasi, C. Kübel, T. Brezesinski, S. S. H. Bhattacharya, H. H. Hahn, et al., *Nature Communications* **9**, 3400 (2018).
 - ³⁹ H. Kawaji, T. Oka, T. Tojo, T. Atake, A. Hirano, and R. Kanno, *Solid State Ionics* **152-153**, 195 (2002), ISSN 0167-2738, URL <http://www.sciencedirect.com/science/article/pii/S0167273802003004>.
 - ⁴⁰ M. Abbate, F. M. F. de Groot, J. C. Fuggle, A. Fujimori, Y. Tokura, Y. Fujishima, O. Strebel, M. Domke, G. Kaindl, J. van Elp, et al., *Phys. Rev. B* **44**, 5419 (1991), URL <https://link.aps.org/doi/10.1103/PhysRevB.44.5419>.
 - ⁴¹ M. A. van Veenendaal and G. A. Sawatzky, *Phys. Rev. B* **50**, 11326 (1994), URL <https://link.aps.org/doi/10.1103/PhysRevB.50.11326>.
 - ⁴² L. Montoro, M. Abbate, E. Almeida, and J. Rosolen, *Chemical Physics Letters* **309**, 14 (1999), ISSN 0009-2614, URL <http://www.sciencedirect.com/science/article/pii/S0009261499006508>.
 - ⁴³ V. Bisogni, S. Catalano, R. J. Green, M. Gibert, S. Raoul, Y. Huang, V. N. Strocov, P. Zubko, S. Balandeh, J.-M. Triscone, et al., *Nature Communications* **7**, 13017 (2016).